Surface & Coatings Technology 474 (2023) 130083

Contents lists available at ScienceDirect

Surface & Coatings Technology

journal homepage: www.elsevier.com/locate/surfcoat

Full Length Article

Ultra-low wear of titanium alloy surface under lubricated conditions achieved by laser texturing and simultaneous nitriding

Chao Wang [a], Hu Huang [a,*], Haoxiang Wu [a], Jing Hong [a], Lin Zhang [b], Jiwang Yan [b]

[a] Key Laboratory of CNC Equipment Reliability, Ministry of Education, School of Mechanical and Aerospace Engineering, Jilin University, Changchun, Jilin 130022, China

[b] Department of Mechanical Engineering, Faculty of Science and Technology, Keio University, Yokohama 223-8522, Japan

ARTICLE INFO

Keywords:
Titanium alloy
Laser nitriding
Surface texturing
Tribological properties

ABSTRACT

Titanium and its alloys are widely used in aerospace and biomedical fields but suffer from poor tribological properties. Surface coating and texturing have proven to be effective ways for improving tribological properties. However, integrating these methods may introduce complexity and increased costs. In this study, laser nitriding and surface texturing were simultaneously achieved on Ti6Al4V surface via a nanosecond pulse laser. The tribological properties of textured surfaces under lubricated conditions were investigated, and the wear mechanism was discussed. Experimental results showed significant improvements in the tribological properties, including a smaller and stable coefficient of friction (COF) and a remarkable 99.3 % reduction in wear rate. This study provides valuable insights for improving the tribological properties of titanium alloys, benefiting industrial and biomedical applications.

1. Introduction

Titanium and its alloys are widely employed in aerospace components and biomedical implants, owing to their superior specific strength, favorable biocompatibility, and excellent corrosion resistance [1–3]. Nonetheless, their poor tribological properties hinder their suitability for contact parts, such as bearings or bolts, as they are susceptible to wear during operation [4,5]. Moreover, the use of titanium alloys as biological implants can result in wear 0debris and diffusion of metal V elements, thereby leading to aseptic loosening and inflammatory reactions, ultimately causing implant failure [6,7]. Therefore, enhancing the wear resistance of titanium alloys is critical for their industrial and medical applications.

Coating technologies have been proven to effectively enhance the wear resistance of material surfaces. Among them, titanium nitride (TiN) is a preferred coating material for titanium alloys due to its exceptional hardness and wear resistance, chemical stability, and superior biocompatibility compared to titanium alloys [8–10]. Laser nitriding, in comparison to conventional coating preparation methods such as thermal spraying, and physical/chemical vapor deposition (P/CVD), offers several advantages including clean, efficiency, precision processing, and high repeatability. Moreover, the TiN layer formed through strong metallurgical bonding between N atoms and Ti-based substrate at high temperature and pressure avoids delamination of coatings from the substrate. Vadiraj et al. reported that the failure of PVD-TiN coating on titanium alloys was primarily attributed to delamination and abrasive wear [11]. In contrast, laser nitriding can achieve a maximum nitriding depth of up to 30 μm, with microstructures evolving in the depth direction [12]. In a comparative study by Torrent et al., both PVD-TiN coating and laser-nitrided layer on titanium surfaces exhibited similar friction coefficients (0.6–0.8); however, the latter showed higher resistance to fretting wear [13]. Furthermore, several studies [14,15] demonstrated that laser nitriding not only improves wear resistance and hardness but also exhibits antibacterial adhesion properties. Therefore, laser nitriding is the preferred approach for improving the wear resistance of titanium alloy surfaces, whether for industrial or biomedical applications.

Surface texturing is an effective and controllable means for improving the tribological properties of mechanical surfaces. Well-designed surface textures can act as micro-bearing to increase the dynamic pressure between the friction pairs [16], store lubricant [17], and trap debris [18] generated during the friction process. For instance, Xing et al. investigated the effects of surface textures on the tribological behavior of Si_3N_4/TiC ceramic and found that surface textures played a

* Corresponding author.
E-mail address: huanghu@jlu.edu.cn (H. Huang).

https://doi.org/10.1016/j.surfcoat.2023.130083
Received 28 July 2023; Received in revised form 22 September 2023; Accepted 7 October 2023

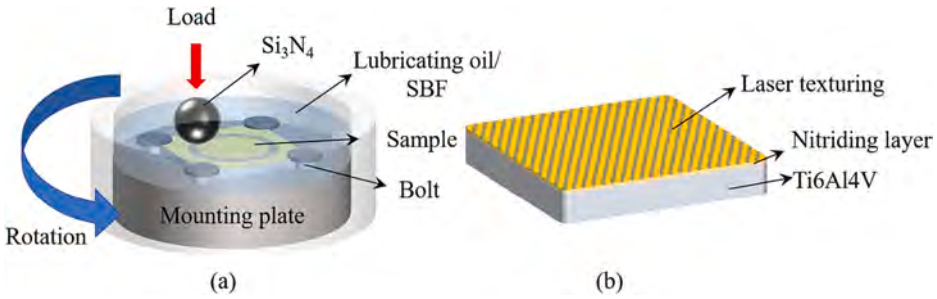

Fig. 1. (a) The ball-on-disc wear test system and (b) schematic of surface nitriding and texturing on the Ti6Al4V surface.

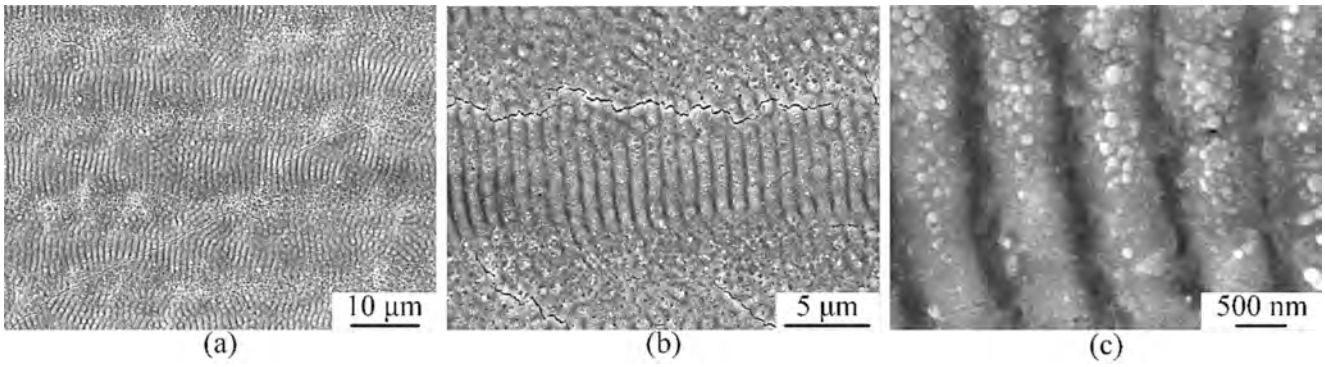

Fig. 2. SEM morphologies of the laser-irradiated surface with different magnifications.

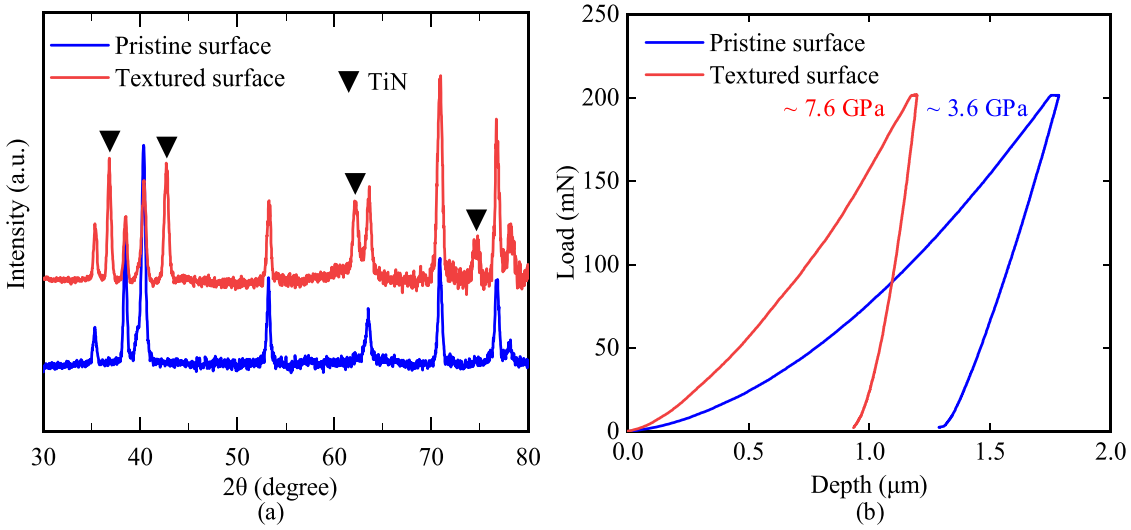

Fig. 3. (a) XRD patterns and (b) load-depth curves of the pristine and textured surfaces.

crucial role in capturing debris and maintaining the lubricating film [19]. Wang et al. conducted a comparative analysis of the tribological mechanism of micro/meso/macroscopic textures under different friction conditions [20]. Mao et al. reviewed the laser surface texturing (LST) techniques, including laser direct ablation, interference, and shock peening, on the engineering materials and highlighted that combining LST with coating or post-treatment could further improve their durability. Therefore, composite processing techniques that integrate LST with other techniques are increasingly employed to enhance the tribological properties of material surfaces. For example, Wang et al. used plasma nitriding and LST to enhance the vacuum tribological properties of titanium alloys [21]. Zhao et al. combined LST and gas nitriding to improve the tribological properties, cyto-biocompatibility, and anti-inflammatory ability of the Ti6Al4V surface [22]. Niu et al. utilized the duplex-treatment of thermal oxidation and LST to maximize the tribological properties of titanium alloys [23].

Compared to a single texturing or nitriding process, composite technologies offer undeniable advantages in improving the tribological properties of titanium alloys. However, combining these separation technologies would introduce complexity and increase the costs for practical applications. In our previous study, simultaneous laser nitriding and surface texturing were achieved on the Ti6Al4V surface via nanosecond pulse laser, improving the surface hardness and scratching characteristics [24]. In this study, the tribological behavior of textured

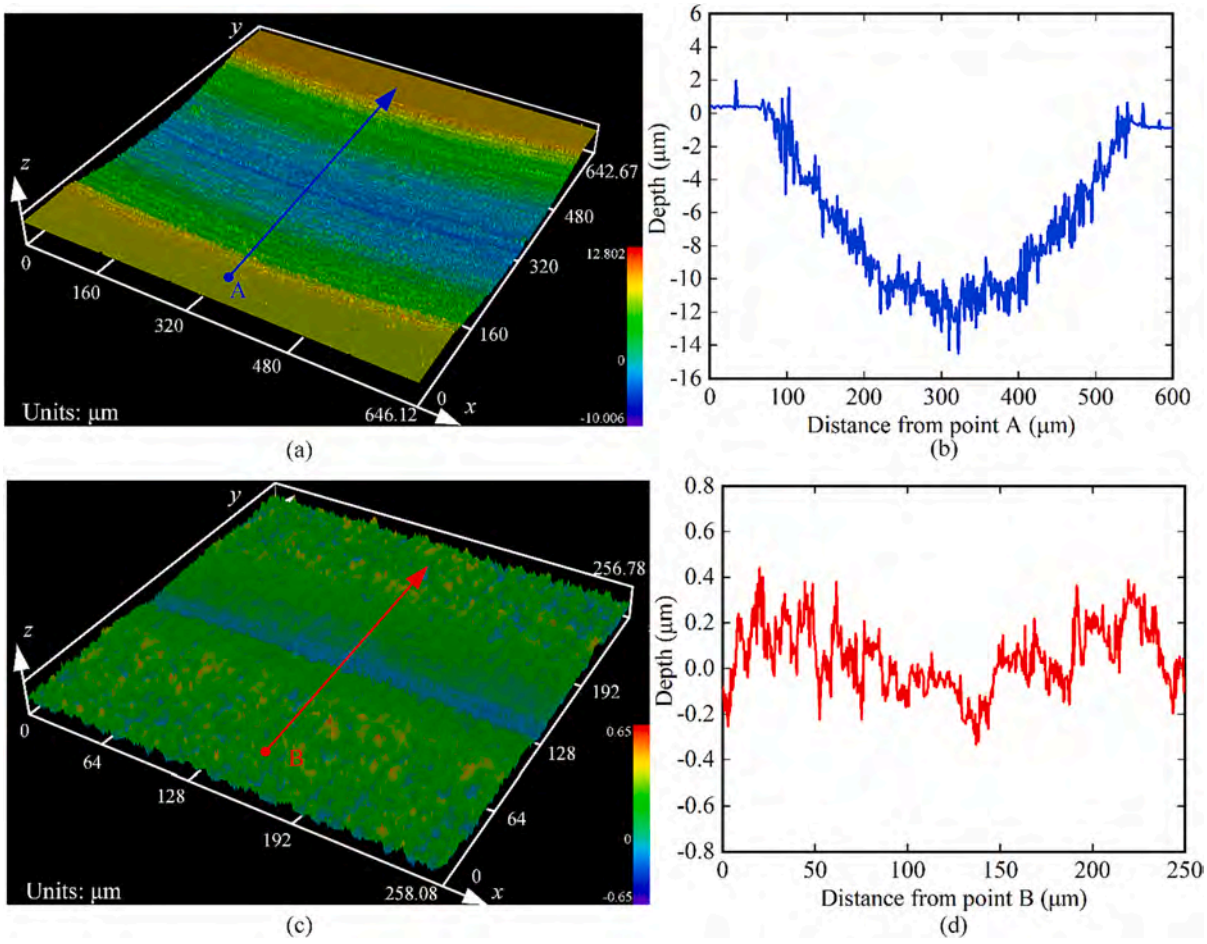

Fig. 4. 3D topographies and corresponding cross-sectional profiles of the worn scars on (a, b) the pristine and (c, d) textured surfaces under oil lubrication.

surfaces under lubricated conditions is further investigated, and the wear mechanism is discussed and analyzed accordingly.

2. Materials and methods

2.1. Materials

Ti6Al4V with dimensions of 20 mm × 20 mm × 3 mm was used as the substrate material. The surface of the samples was ground with #400, #800, #1500, and #3000 SiC sandpapers, and then polished to a mirror finish with W0.5 diamond abrasive paste. Finally, the samples were sonicated with acetone for 15 min and dried at room temperature.

2.2. Simultaneous laser nitriding and surface texturing

A nanosecond fiber laser (SP-050P-A-EP-Z-F-Y, SPI, UK) was employed to simultaneously achieve nitriding and surface texturing. The laser energy has a Gaussian energy distribution (TEM_{00} mode, $M_2 < 1.6$) with a beam diameter of ~43 μm. The laser pulse width is 7 ns and the central wavelength is 1064 nm. To ensure the laser nitriding process, the experiments were carried out under a nitrogen atmosphere at a pressure of 0.05 MPa. According to previous experimental results [25], the surface textures (laser-induced periodic surface structure, LIPSS) were created on the Ti6Al4V surface under the selected laser parameters (laser power: 4.46 W, scanning speed: 10 mm/s, repetition frequency: 700 kHz, intervals between two adjacent scanning lines: 10 μm).

2.3. Tribological testing

The tribological performance of the pristine and textured samples was tested using a ball-on-disc rotary wear tester (HT-1000, Lanzhou Zhongke Kaihua Technology Development Co., Ltd., China). A load of 1.96 N was applied through a ceramic ball (Si_3N_4, Φ5 mm) to the sample. The sample was rubbed against the ceramic ball at a sliding speed of 31.4 mm/s (100 rpm) for 30 min. Fig. 1 illustrates the ball-on-disc wear test system employed in this study. A ceramic ball, subjected to a 200 g weight, is loaded onto the sample which is bolted to a mounting plate rotating by a motor. The experiments were conducted under lubrication conditions in oil (Hotolube, China) and simulated body fluids (SBF), respectively. The selection of lubricants depends on two typical applications of titanium alloys, engineering applications and biomedical applications. To ensure constant lubrication during the wear test, the lubricating oil or SBF level is maintained at 1–2 mm above the sample. The sliding speed is set at 100 rpm to prevent the lubricant from being thrown out. The wear rate could be calculated by the formula: $\omega = V / (S * P)$, where ω is the wear rate, V is the wear volume, S is the sliding distance and P is the applied load. The tests were repeated three times for each sample to ensure the accuracy of the results. The tribological behavior of textured surfaces under lubricating oil/SBF is analyzed in detail below.

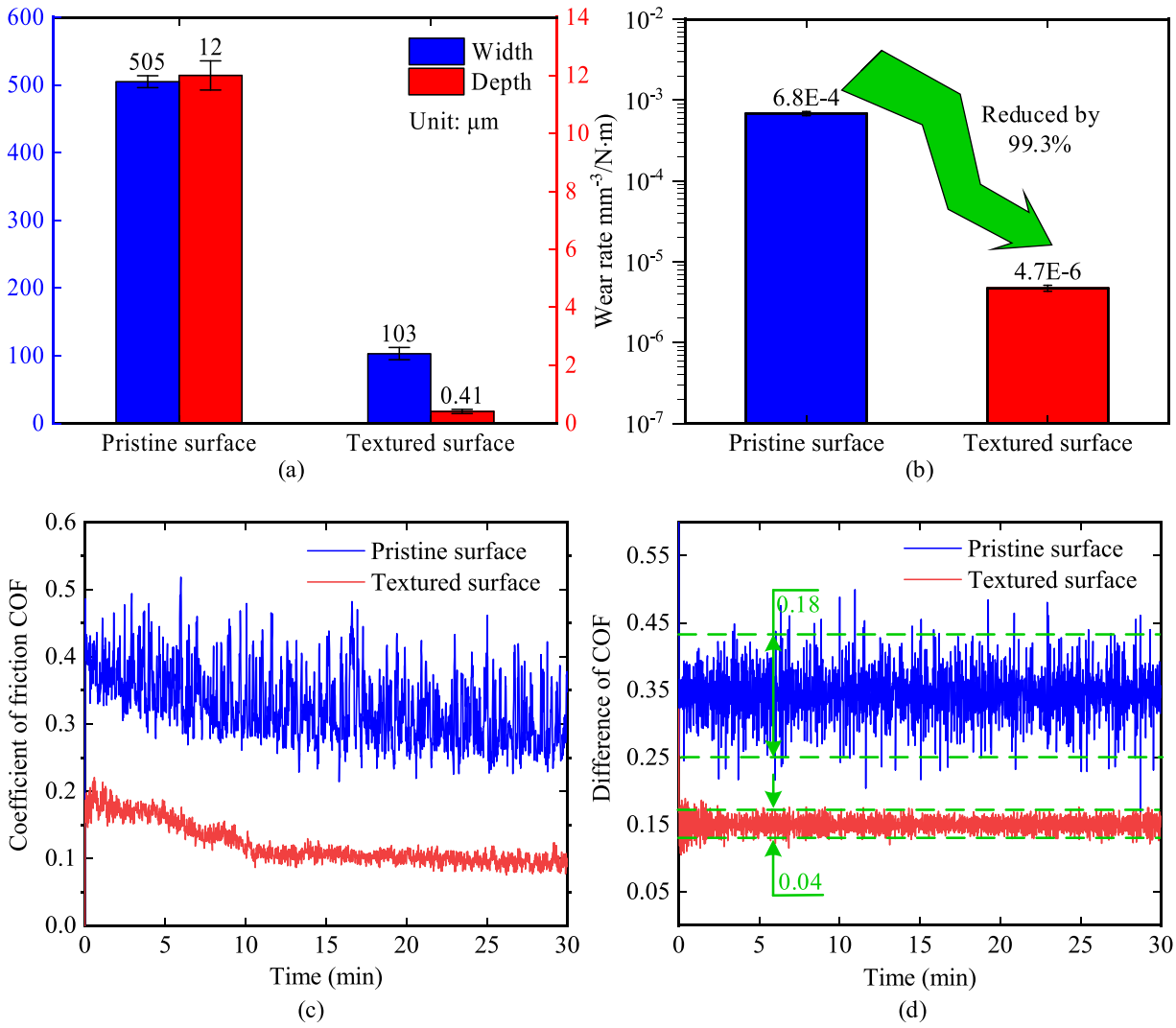

Fig. 5. (a) Width and depth of the worn scars, (b) wear rate, (c) COF curves and (d) difference of COF on the pristine and textured surfaces under oil lubrication.

2.4. Characterizations

The crystal phases of the pristine and textured samples were characterized by an X-ray diffractometer (XRD, D8 Discover, Bruker, Germany). The surface hardness of the pristine and textured samples was measured by a nanoindentation instrument (DUH-211S, SHIMADZU, Japan). The applied load and loading rate were 200 mN and 10 mN/s, respectively. The wear morphologies were observed by a scanning electron microscope (SEM, JSM-IT500A, JEOL, Japan) and a laser scanning confocal microscope (LSCM, OLS5100, Olympus, Japan). The element distribution of the worn surfaces was detected by using an energy dispersive spectroscopy (EDS, EX-74600U4L2Q, JEOL, Japan).

3. Results and discussion

3.1. Surface characterizations

Fig. 2 presents the SEM morphologies of the laser-irradiated surface, which is dominated by LIPSS with a period of approximately 0.98 μm and a height of around 100 nm. A comprehensive investigation on the evolution of LIPSS has been detailed reported in our previous study [25]. The irradiated surface appears uniformly flat, and the distribution of LIPSS demonstrates a relatively regular pattern, which suggests that the surface textures (LIPSS) are well introduced on the Ti6Al4V surface. Fig. 3 illustrates the XRD patterns and load-depth curves of both the pristine and textured surfaces. As depicted in Fig. 3(a), the textured surface exhibits the distinct TiN peaks compared to the pristine surface, which indicates a significant laser nitriding on the textured surface. As shown in Fig. 3(b), the results of the nanoindentation test show that the surface hardness of the textured surface reaches ~7.6 GPa due to the role of laser nitriding, which is significantly higher than that of the pristine surface (~3.6 GPa). The above experimental results show that laser nitriding and surface texturing have been simultaneously achieved on the Ti6Al4V surface.

3.2. Oil lubrication

Fig. 4 depicts the three-dimensional (3D) topographies as well as the corresponding cross-sectional profiles of the worn scars on both the pristine and textured surfaces under oil lubrication. The pristine surface exhibits large and deep worn scars, and the textured surface demonstrates shallow worn scars, implying the protective effect of laser nitriding and texturing. Fig. 5(a) and (b) presents the statistical results for the width, depth, and wear rate. From Fig. 5(a), it can be seen that the width and depth of wear scars on the pristine surface reach 505 μm and 12 μm, respectively. While, the width and depth of wear scars on the

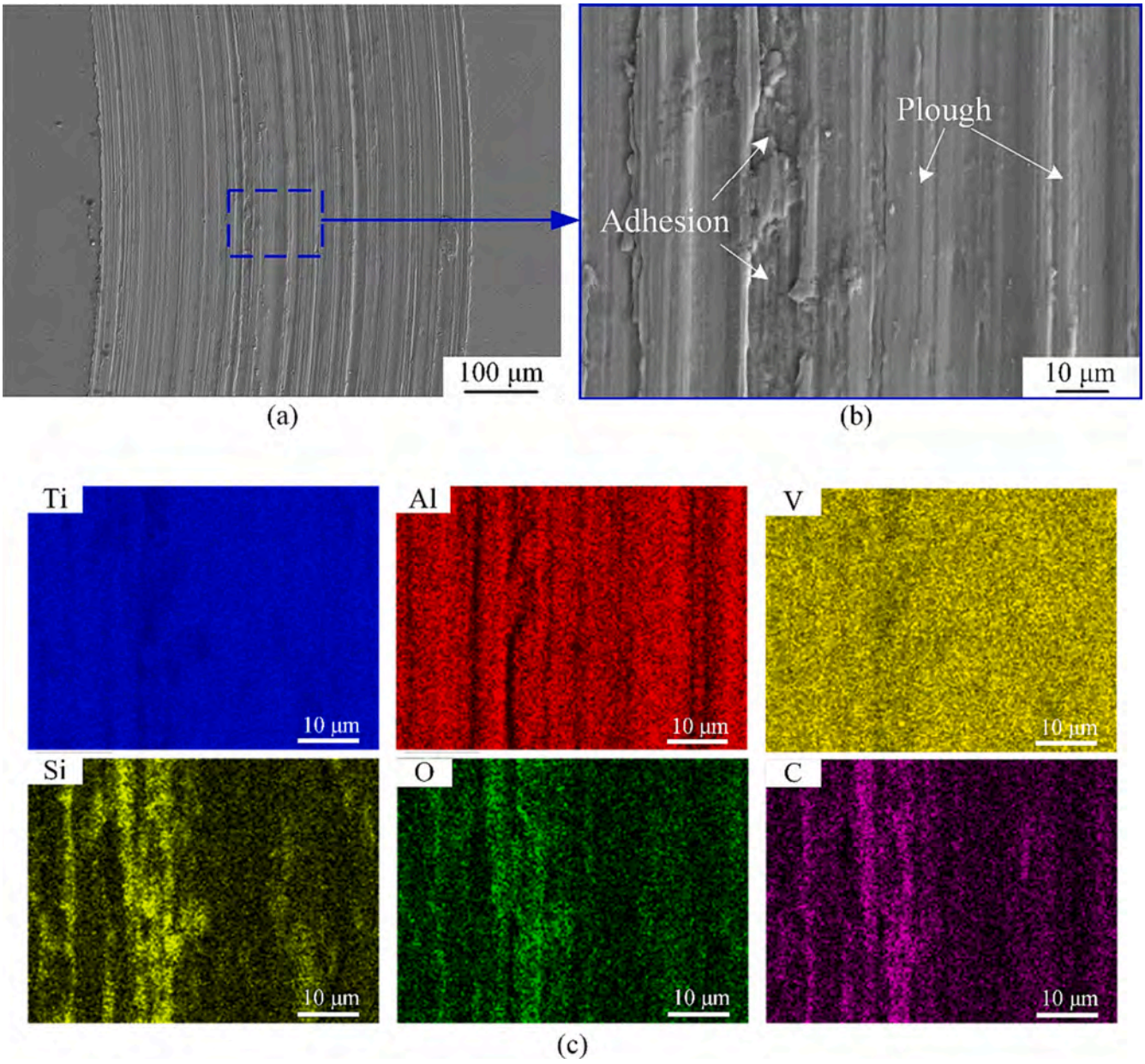

Fig. 6. (a, b) SEM morphologies of the worn scars on the pristine surface under oil lubrication. (c) EDS mapping corresponding to (b).

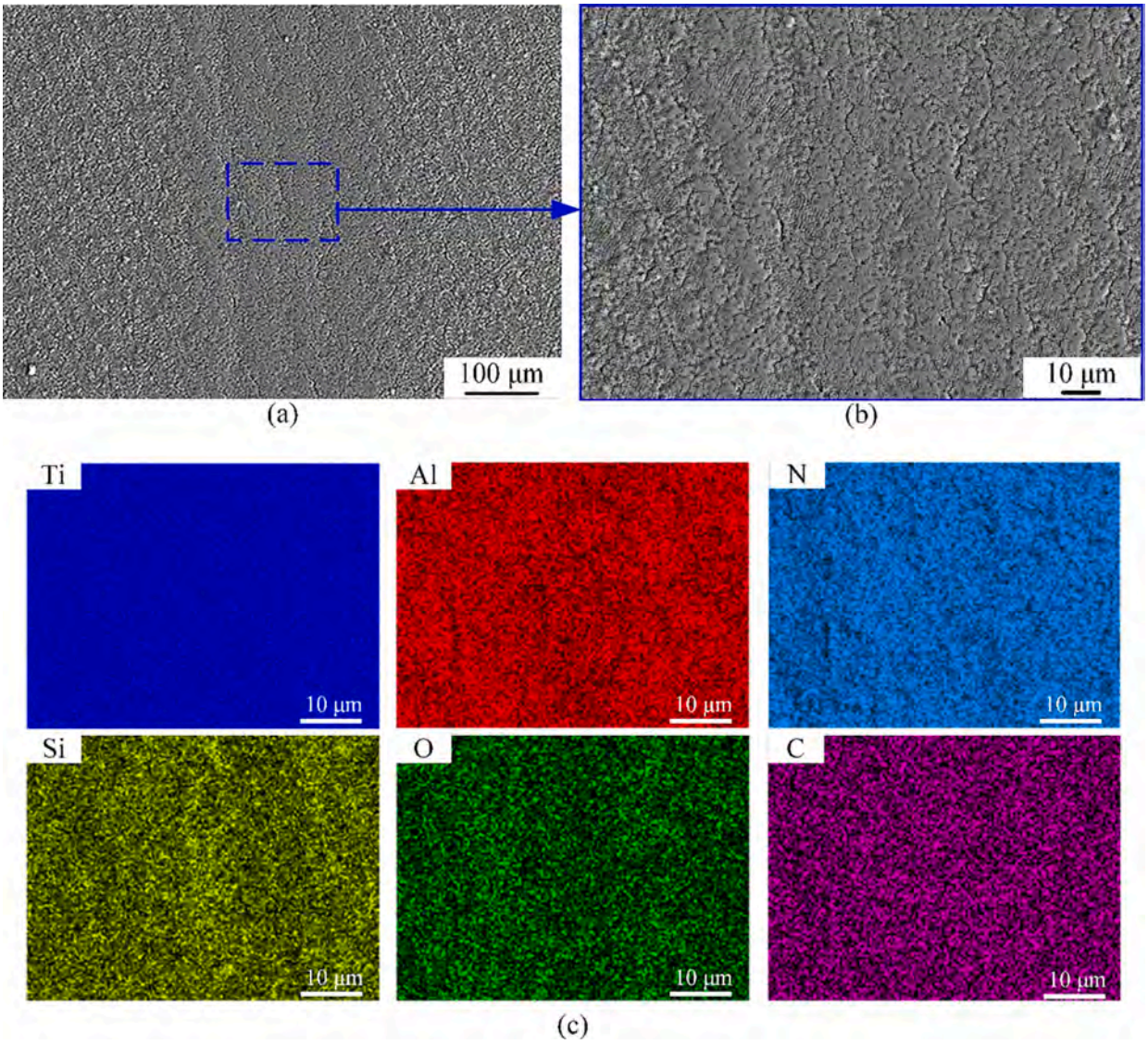

Fig. 7. (a, b) SEM morphologies of the worn scars on the textured surface under oil lubrication. (c) EDS mapping corresponding to (b).

Table 1
Element content of the pristine surface and textured surface.

Element (at. %)	Ti	Al	V	Si	C	O	N
Pristine surface	61.56 ± 0.12	6.83 ± 0.06	2.63 ± 0.05	1.06 ± 0.02	12.3 ± 0.07	15.7 ± 0.09	0
Textured surface	44.23 ± 0.11	2.50 ± 0.07	2.53 ± 0.05	0.27 ± 0.01	7.03 ± 0.06	10.43 ± 0.08	33.03 ± 0.10

textured surface are reduced to 103 μm and 0.41 μm respectively, as can be seen in Fig. 5(b). Furthermore, the wear rate for the pristine surface is 6.8×10^{-4} mm^{-3}/N·m, and the wear rate for the textured surface is only 4.7×10^{-6} mm^{-3}/N·m, indicating a remarkable 99.3 % reduction in the wear rate of the titanium alloy surface after simultaneous laser nitriding and surface texturing. Figs. 5(c) and (d) display the images of the coefficient of friction (COF) and the difference of COF, respectively. The difference of COF is defined as the value of the latter minus the former in COF series, which is used to assess the stability of the wear process. The COF value for the pristine surface remains consistently around 0.31, while for the textured surface, it is only approximately 0.1. Additionally, the difference of COF for the textured surface is 0.04, and it is 0.18 for the pristine surface. During the wear process, the continuous collision between the Ti6Al4V surface and the hard Si3N4 ball results in material removal, with the generation of debris. This continuous peeling-off debris induces fluctuations in the COF, resulting in a relatively high "difference of COF" (approximately 0.18) for the pristine surface. In contrast, due to the beneficial nitriding effect and the presence of surface textures, the textured surface exhibits enhanced resistance to material peeling [9]. Moreover, the surface textures act as effective traps, minimizing the accumulation of debris [18]. As a result, the COF remains stable, with a low "difference of COF" (approximately 0.04) during the wear process. These findings further confirm that the textured surface exhibits enhanced wear resistance during the friction process.

Figs. 6 and 7 present the SEM morphologies as well as the corresponding EDS mapping of worn scars on both the pristine and textured surfaces. It is worth noting that the oil-lubricated worn samples are ultrasonically cleaned using acetone to remove the residual lubricant. This

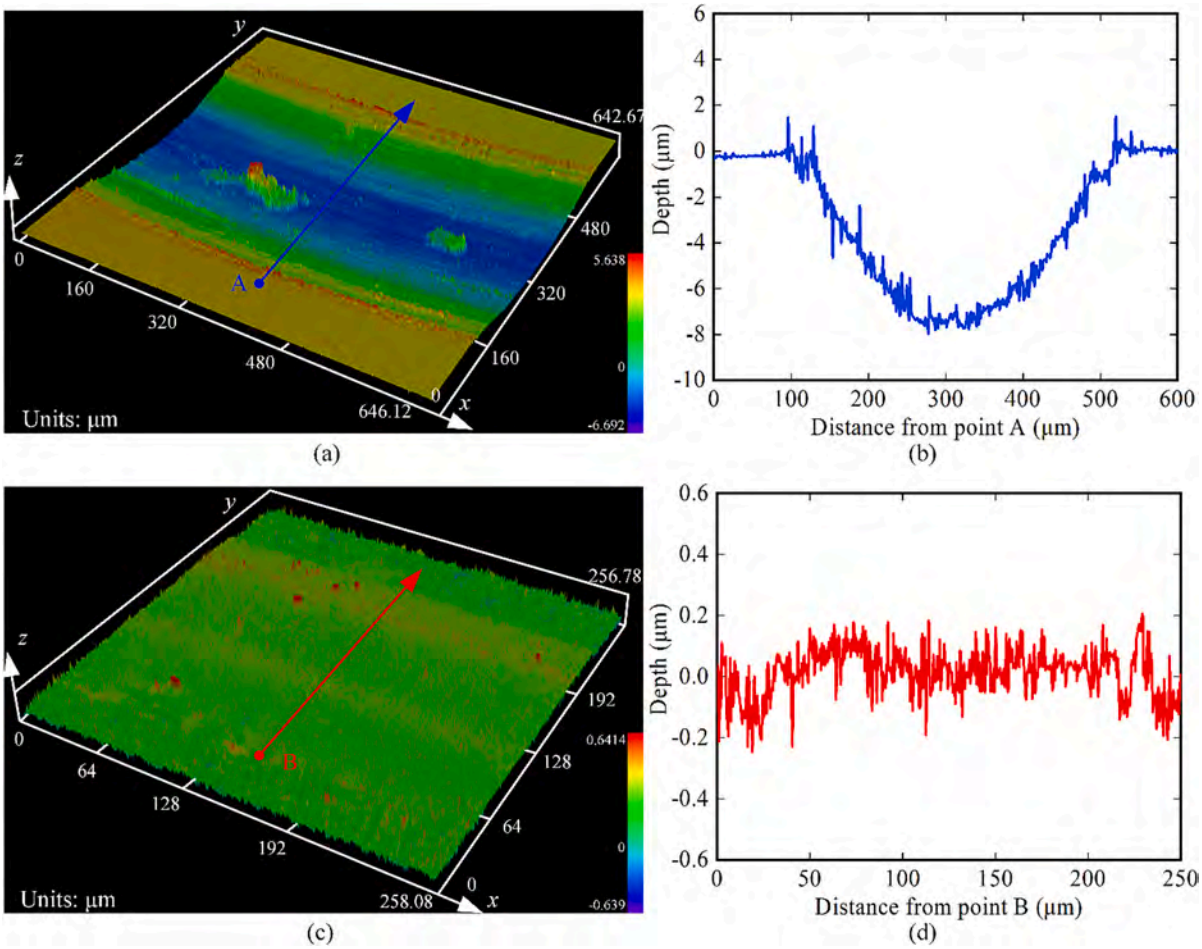

Fig. 8. 3D topographies and corresponding cross-sectional profiles of the worn scars on (a, b) the pristine surface and (c, d) textured surface under SBF lubrication.

process removes some debris produced during friction process, thereby making it invisible in the SEM morphologies. However, obvious plough could be observed on the worn scars of the pristine surface, which indicates that the primary wear mechanism is abrasive wear. EDS mapping results reveal the presence of Si, C, and O elements in certain regions, which originate from the transfer of Si_3N_4 ceramic balls and residual lubricant, demonstrating the occurrence of adhesion wear mechanism. As depicted in Fig. 7, the worn scars of the textured surface are not obvious, but ploughing is evident, indicating the abrasive wear mechanism. According to the element content in Table 1, the worn scars of the textured surface contain very little Si element, suggesting the absence of adhesion behavior of the Si_3N_4 ceramic balls.

3.3. SBF lubrication

Fig. 8 showcases the 3D topographies and the corresponding cross-sectional profiles of worn scars on both the pristine and textured surfaces under SBF lubrication. It can be observed that the pristine surface is heavily worn, while the textured surface shows minimal wear. Figs. 9 (a) and (b) show the statistical results of the width, depth, and wear rate. As depicted in Fig. 9(a), the width and depth of the worn scars on the pristine surface reach 400 μm and 7.97 μm, respectively. While for the textured surface, the width and depth of worn scars are only 174 μm and 0.13 μm, respectively. As a result, the wear rate is sharply reduced from 3.9×10^{-4} mm^{-3}/N·m on the pristine surface to 2.5×10^{-6} mm^{-3}/N·m on the textured surface, achieving a remarkable reduction of 99.3 %. Fig. 9(c) and (d) shows the images of COF and the difference in COF. The COF of the pristine surface remains stable at approximately 0.3, whereas for the textured surface, it is approximately 0.2. The difference of COF for the pristine surface is 0.2, whereas for the textured surface, it is only 0.06. These results show that textured surface still exhibits enhanced tribological behavior under SBF lubrication conditions.

Fig. 10(a)–(c) presents the SEM morphologies of the worn scars on the pristine surface, where visible plough and debris are observed, indicating its abrasive wear mechanism. Besides, Ca, Cl, P, and Si elements are detected on the debris by EDS analysis in Fig. 10(d), which is derived from the residual SBF and the transfer of Si_3N_4 ceramic balls. Fig. 11 presents the SEM morphologies of the worn scars on the textured surface, revealing two main features: the worn textured surface depicted in Fig. 11(b) as well as the fragmented surface depicted in Fig. 11(c). Based on the results of EDS analysis at point 2 and point 3, more Ca and P elements are enriched at point 2 compared to point 3. SBF is a supersaturated solution containing a substantial concentration of calcium (Ca) and phosphorus (P) ions, mimicking the composition of natural biological fluids. During the wear testing process, several phenomena come into play. First, as material peeling occurs, partially detached material from the Ti6Al4V surface is introduced into the SBF solution. Additionally, under the testing conditions, the SBF solution may undergo volatilization. These combined factors contribute to the precipitation of Ca and P ions within the SBF onto the worn surfaces. As a consequence, these ions adhere to the worn scars, forming deposits and leading to the appearance of a fragmented surface. This adhesion behavior is influenced by the chemical composition of the solution and its interaction with the worn surface. Therefore, it is assumed that the

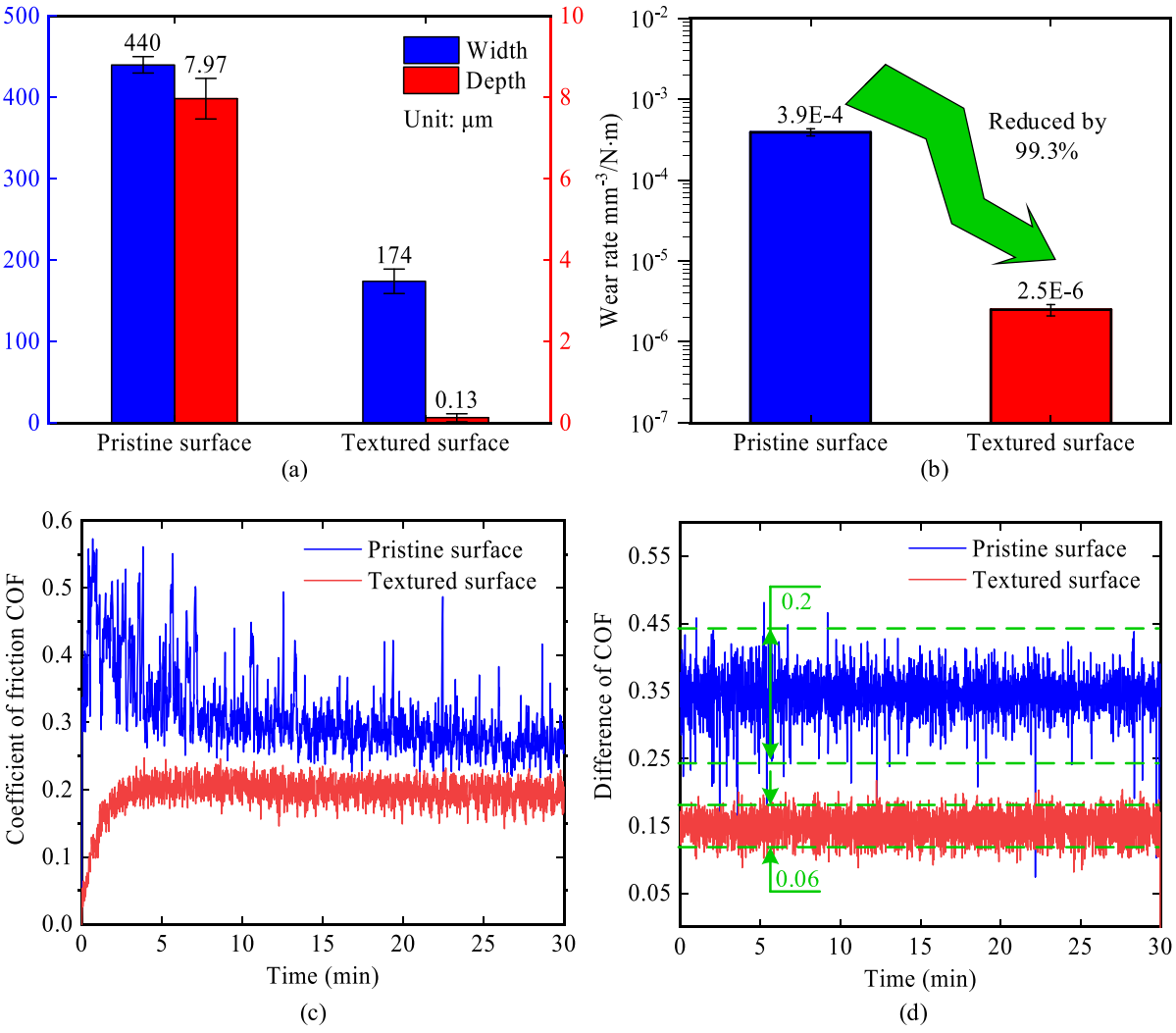

Fig. 9. (a) Width and depth of worn scars, (b) wear rate, (c) COF curves and (d) difference of COF on the pristine surface and textured surface under SBF lubrication.

fragmented surface originates from the adhesion of residual SBF during the wear process. While for the worn textured surface, the wear is very slight, with only a few debris, proving the abrasive wear mechanism.

To explore the individual effect of nitriding or texturing on the wear mechanism, the wear tests were conducted on the textured and then polished surface. The aim of mechanical polishing is to eliminate the LIPSS from the modified surface. Fig. 12(a) and (b) presents the 3D topography and corresponding cross-sectional profile of the worn scar under oil lubrication. The depth and width of the worn scar are about 0.3 and 110 μm, indicating a very low wear rate (3.7×10^{-6} mm^{-3}/N·m). Fig. 12(c) and (d) displays the images of the COF and the difference of COF, respectively. Compared to the textured surface (0.04), the COF curve exhibits a pronounced increase and significant fluctuations, with the difference of COF increasing to 0.18. This phenomenon could be related to the failure of oil film and the delayed removal of wear particles. However, SEM analysis (refer to Figs. 6 and 7) does not reveal the presence of wear particles, likely due to their removal during subsequent cleaning processes.

Therefore, wear tests were further performed on the textured surface as well as the textured and then polished surface without lubrication. The corresponding results of SEM morphologies and EDS mappings are shown in Figs. 13 and 14. As shown in Fig. 13(a), obvious plough could be observed on the worn scar of the textured surface, which indicates that the primary wear mechanism is abrasive wear. EDS mapping in Fig. 13(d) and (e) indicates the presence of substantial amounts of Si and O elements within the worn scar, indicating the oxidative wear mechanism. As shown in Fig. 13(c), massive debris is present within the LIPSS, proving the debris trapping effect of the textured surface [26]. Conversely, for the textured and then polished surface, only limited Si and O elements remain within the worn scar, as observed in Region A of Fig. 14(a). Besides, some bulk wear particles enriched with Si element similar to those in Region B are observed on both sides of worn scars, indicating the material transfer of the Si_3N_4 ceramic balls during the wear process. Furthermore, Fig. 14(c) shows the presence of fine wear particles, primarily concentrated on the residual LIPSS (highlighted within the red circle), as opposed to the smooth surface. This observation further confirms the debris trapping effect conferred by LIPSS.

The above experimental results demonstrate that under lubricated conditions (oil/SBF), the textured surface exhibits a significantly reduced wear rate and a smoother COF compared to the pristine surface. Fig. 15 illustrates the wear mechanisms on both the pristine surface and textured surface of the Ti6Al4V. As shown in Fig. 15(a), the hard Si_3N_4 ball and Ti6Al4V slide against each other, resulting in the detachment of the material, thus generating debris. The accumulated debris, unable to be timely removed, further intensifies the wear behavior. Fig. 15(b) shows the wear mechanism of the textured surface. Through

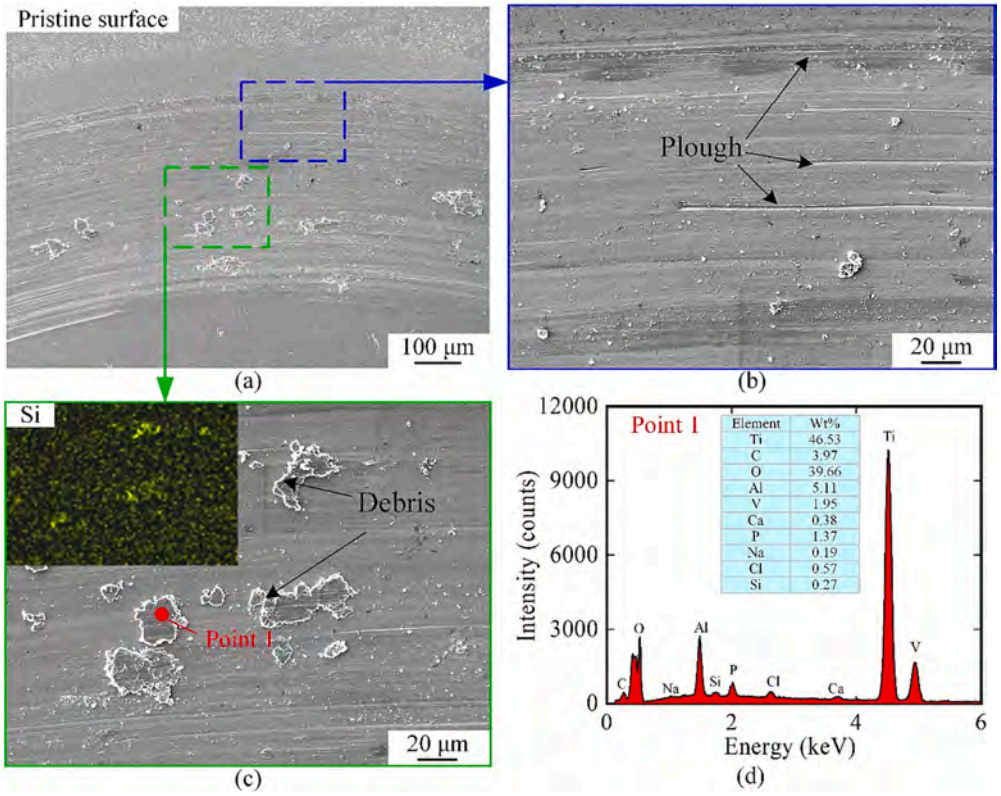

Fig. 10. (a)–(c) SEM morphologies of worn scars on pristine surface under SBF lubrication. (d) EDS composition analysis of point 1 in (c).

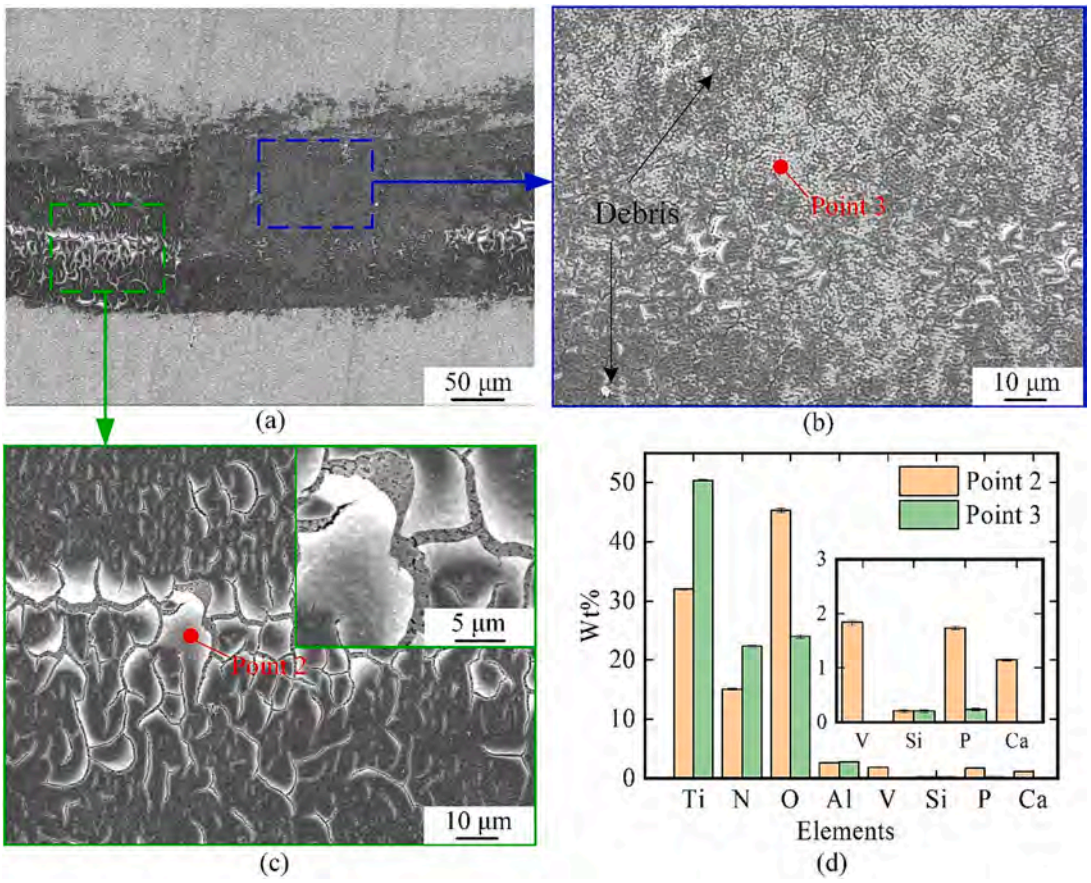

Fig. 11. (a)–(c) SEM morphologies of worn scars on textured surface under SBF lubrication. (d) EDS analysis at point 2 and 3.

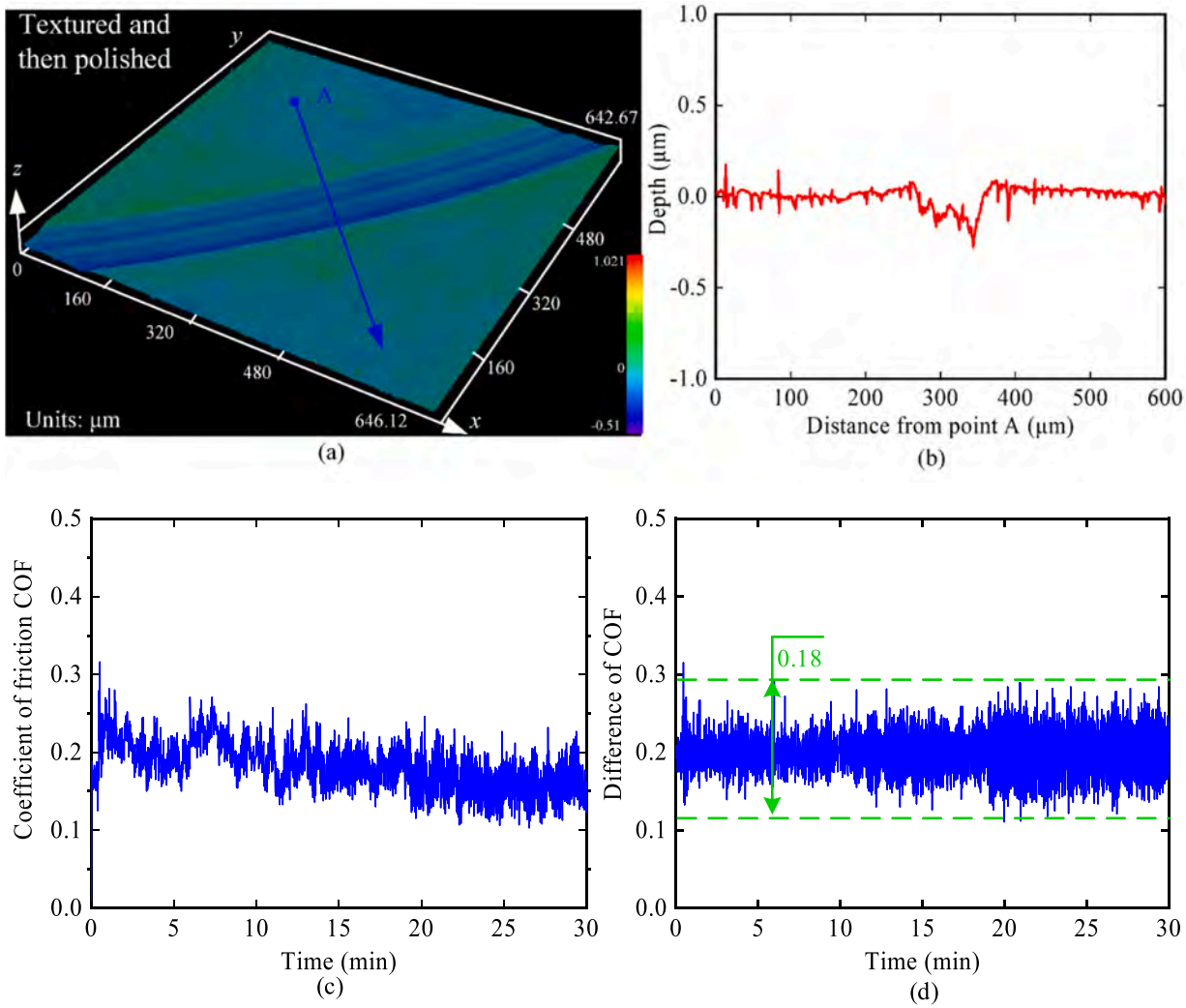

Fig. 12. (a, b) 3D topography and corresponding cross-sectional profile of the worn scar, (c) COF curves and (d) difference of COF on the textured and then polished surface under oil lubrication.

simultaneous laser nitriding and texturing, a hard nitriding layer and LIPSS structures are formed on the Ti6Al4V surface. Compared to the pristine surface, the textured surface exhibits minimal debris [26,27]. During friction processes, the hard nitriding layer is more resistant to wear and detachment [9], while the surface textures effectively trap the wear debris, which can effectively reduce abrasive and adhesive wear [18]. Besides, under lubricated conditions, the surface textures can store lubricants and form an oil film during the friction process [17]. Consequently, the textured surface demonstrates superior tribological properties compared to the pristine surface.

4. Conclusions

In conclusion, the textured Ti6Al4V surface, achieved through simultaneous laser nitriding and texturing, demonstrated superior tribological properties under both oil and SBF lubrication, with reduced wear rates and smoother coefficient of friction (COF). The findings can be summarized as follows:

(1) Under oil-lubricated conditions, the COF of the textured surface is more stable and reduced from 0.31 to 0.1, and the wear rate is reduced by 99.3 %. The primary wear mechanism observed on the pristine surface is abrasive wear and slight adhesion wear, evidenced by the presence of plough and residual elements on the worn scars. In contrast, the textured surface indicates the absence of adhesion behavior.

(2) Under SBF-lubricated conditions, the textured surface also exhibits a smaller and more stable COF (~0.2), and the wear rate is also reduced by 99.3 %. The pristine surface shows visible ploughing and debris, indicating abrasive wear, while the textured surface exhibits slight wear with minimal debris. Besides, the worn scars on the textured exhibit the adhesion behavior of residual SBF.

(3) Compared to the pristine Ti6Al4V surface, the presence of a hard nitriding layer improves wear resistance and reduces debris accumulation, and the surface textures facilitate debris capture and lubricant retention. The synergy between the two contributes to the excellent tribological properties of Ti6Al4V.

Overall, these findings demonstrate that composite technologies (nitriding and texturing) offer the improved tribological properties of Ti6Al4V, making it a promising approach for enhancing the performance of titanium alloys.

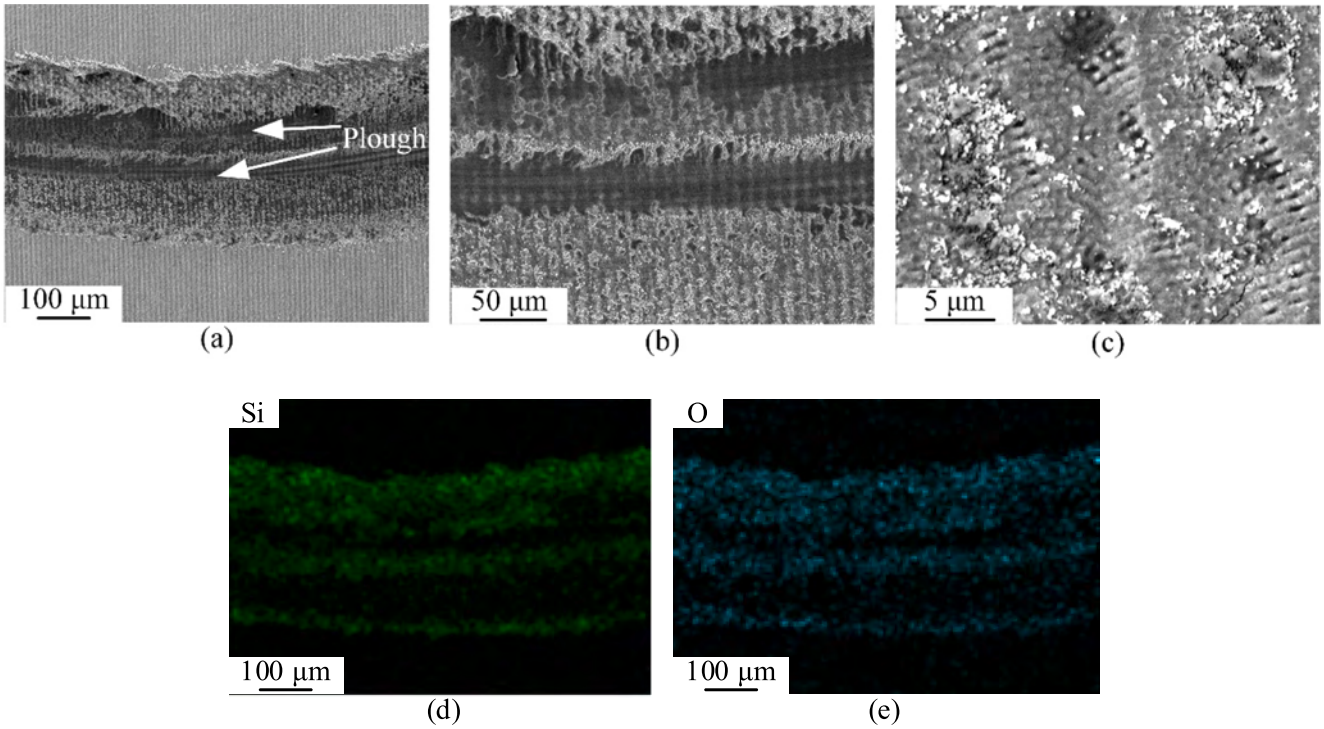

Fig. 13. (a)–(c) SEM morphologies of the worn scar on the textured surface without lubrication. (d) and (e) EDS mappings corresponding to (a).

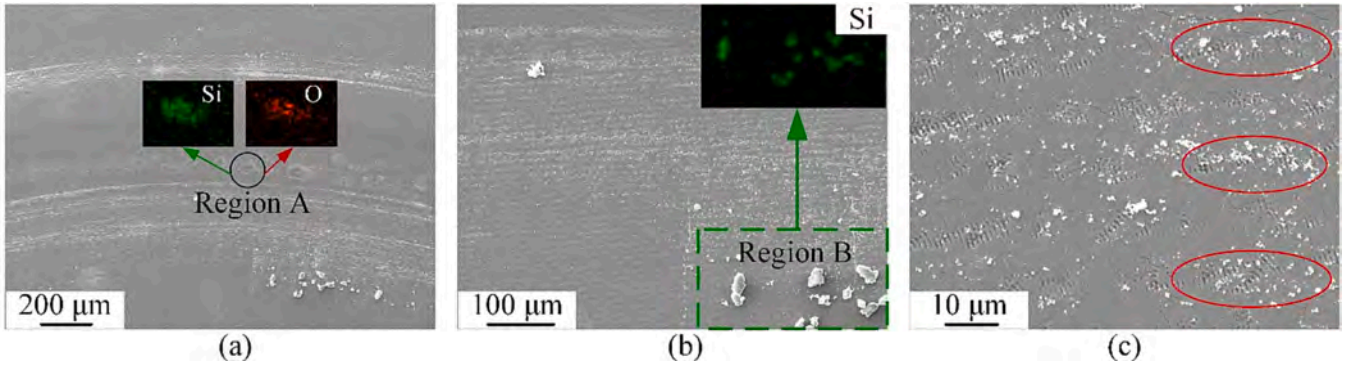

Fig. 14. (a)–(c) SEM morphologies of the worn scar on the textured and then polished surface without lubrication. The insets show the EDS mappings for the corresponding region.

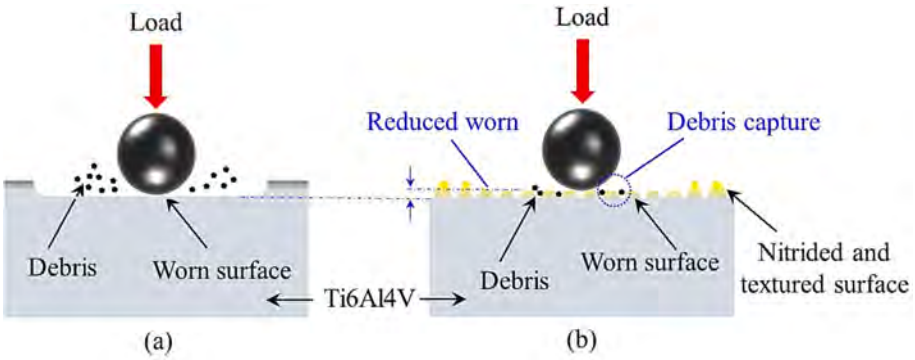

Fig. 15. Wear mechanisms of the (a) pristine surface and (b) textured surface.

CRediT authorship contribution statement

Chao Wang: Investigation, Formal analysis, Data curation, Writing – original draft. **Hu Huang:** Conceptualization, Funding acquisition, Methodology, Resources, Supervision, Writing – review & editing. **Haoxiang Wu:** Investigation, Validation. **Jing Hong:** Investigation. **Lin Zhang:** Investigation. **Jiwang Yan:** Supervision.

Declaration of competing interest

The authors declare that they have no known competing financial interests or personal relationships that could have appeared to influence the work reported in this paper.

Data availability

Data will be made available on request.

Acknowledgements

This work was supported by the Natural Science Foundation of Jilin Province (20220101198JC), the Graduate Innovation Fund of Jilin University (Grant No. 2023CX062), the Opening Project of the Key Laboratory of CNC Equipment Reliability, Ministry of Education, Jilin University (JLU-cncr-202306), and the Fundamental Research Funds for the Central Universities (2023-JCXK-02).

References

[1] D. Banerjee, J.C. Williams, Perspectives on titanium science and technology, Acta Mater. 61 (2013) 844–879.
[2] H.J. Rack, J.I. Qazi, Titanium alloys for biomedical applications, Mater. Sci. Eng. C 26 (2006) 1269–1277.
[3] L.C. Zhang, L.Y. Chen, A review on biomedical titanium alloys: recent progress and prospect, Adv. Eng. Mater. 21 (2019) 1801215.
[4] F. Li, M. Gao, B. Guo, Friction and lubrication mechanism of a new type of anti-magnetic bearing Ti60 titanium alloy material, Res. Phys. 14 (2019), 101827.
[5] H. Yu, Z. Wang, J. Yuan, Loosening and fracture behavior of hybrid titanium-to-steel threaded connection under cyclic loading condition, Eng. Fail. Anal. 142 (2022), 106742.
[6] W. de Souza, S. Gemini-Piperni, L. Grenho, L.A. Rocha, J.M. Granjeiro, S.A. Melo, M.H. Fernandes, A.R. Ribeiro, Titanium dioxide nanoparticles affect osteoblast-derived exosome cargos and impair osteogenic differentiation of human mesenchymal stem cells, Biomater. Sci. 11 (2023) 2427–2444.
[7] L. Freitag, T. Spinell, A. Kroger, G. Wurfl, M. Lauseker, R. Hickel, M. Kebschull, Dental implant material related changes in molecular signatures in peri-implantitis - a systematic review and integrative analysis of omics in-vitro studies, Dent. Mater. 39 (2023) 101–113.
[8] L. Zhang, M. Shao, Z. Wang, Z. Zhang, Y. He, J. Yan, J. Lu, J. Qiu, Y. Li, Comparison of tribological properties of nitrided Ti-N modified layer and deposited TiN coatings on TA2 pure titanium, Tribol. Int. 174 (2022), 107712.
[9] Ş. Danışman, D. Odabaş, M. Teber, The effect of TiN, TiAlN, TiCN thin films obtained by reactive magnetron sputtering method on the wear behavior of Ti6Al4V alloy: a comparative study, Coatings 12 (2022) 1238.
[10] A. Vereschaka, V. Tabakov, S. Grigoriev, N. Sitnikov, N. Andreev, F. Milovich, Investigation of wear and diffusion processes on rake faces of carbide inserts with Ti-TiN-(Ti,Al,Si)N composite nanostructured coating, Wear 416-417 (2018) 72–80.
[11] A. Vadiraj, M. Kamaraj, Fretting fatigue studies of titanium nitride-coated biomedical titanium alloys, J. Mater. Eng. Perform. 15 (2006) 553–557.
[12] X. Zong, H. Wang, J. Li, X. Cheng, Z. Li, H. Tang, Microstructure characterization and evolution mechanism of titanium during laser surface nitriding, Mater. Charact. 190 (2022), 112029.
[13] F. Torrent, L. Lavisse, P. Berger, G. Pillon, C. Lopes, F. Vaz, M.C. Marco de Lucas, Influence of the composition of titanium oxynitride layers on the fretting behavior of functionalized titanium substrates: PVD films versus surface laser treatments, Surf. Coat. Technol. 255 (2014) 146–152.
[14] C.-W. Chan, L. Carson, G.C. Smith, A. Morelli, S. Lee, Enhancing the antibacterial performance of orthopaedic implant materials by fibre laser surface engineering, Appl. Surf. Sci. 404 (2017) 67–81.
[15] X. Chang, G.C. Smith, J. Quinn, L. Carson, C.W. Chan, S. Lee, Optimization of anti-wear and anti-bacterial properties of beta TiNb alloy via controlling duty cycle in open-air laser nitriding, J. Mech. Behav. Biomed. Mater. 110 (2020), 103913.
[16] H. Jia, Z. Zhou, B. Yin, H. Zhou, B. Xu, Effect of compound texture on lubrication and sealing performance of plunger pump, Lubr. Sci. 33 (2020) 43–59.
[17] D.Z. Segu, Y. Chae, S.-J. Lee, C.-L. Kim, Synergistic influences of laser surface texturing and ZrO2-MoDTC hybrid nanofluids for enhanced tribological performance, Tribol. Int. 183 (2023), 108377.
[18] H. Zou, B. Lin, X. Ren, H. Li, Q. Diao, Y. Wang, T. Sui, S. Yan, Particle size effects on efficiency of surface texturing in reducing friction, Tribol. Int. 176 (2022), 107895.
[19] Y. Xing, J. Deng, Z. Wu, H. Cheng, Effect of regular surface textures generated by laser on tribological behavior of Si3N4/TiC ceramic, Appl. Surf. Sci. 265 (2013) 823–832.
[20] Y. Wang, T. Zhou, O. Riemer, J. Heidhoff, M. Li, B. Karpuschewski, S.N. Gorb, C. F. Schaber, Tribological mechanism of micro/meso/macroscopic textured surfaces under different normal forces, relative velocities, and sliding directions, Tribol. Int. 176 (2022), 107708.
[21] M.-Z. Wang, J.-J. Kang, W. Yue, Z.-Q. Fu, L.-N. Zhu, D.-S. She, C.-B. Wang, Effects of combined treatment of plasma nitriding and laser surface texturing on vacuum tribological behavior of titanium alloy, Mater. Res. Express 6 (2019), 066511.
[22] X. Zhao, B. Wang, W. Lai, G. Zhang, R. Zeng, W. Li, X. Wang, Improved tribological properties, cyto-biocompatibility and anti-inflammatory ability of additive manufactured Ti-6Al-4V alloy through surface texturing and nitriding, Surf. Coat. Technol. 425 (2021), 127686.
[23] Y. Niu, X. Pang, C. Song, B. Shangguan, Y. Zhang, S. Wang, Tailoring tribological properties of Ti-Zr alloys via process design of laser surface texturing and thermal oxidation, Surf. Interfaces 37 (2023), 102743.
[24] C. Wang, J. Hong, M. Cui, H. Huang, L. Zhang, J. Yan, The effects of simultaneous laser nitriding and texturing on surface hardness and tribological properties of Ti6Al4V, Surf. Coat. Technol. 437 (2022), 128358.
[25] C. Wang, H. Huang, Y. Qian, Z. Zhang, W. Huang, J. Yan, Nitrogen assisted formation of large-area ripples on Ti6Al4V surface by nanosecond pulse laser irradiation, Precis. Eng. 73 (2022) 244–256.
[26] X. Pan, L. Zhou, D. Hu, W. He, P. Liu, Z. Yu, X. Liang, Superior wear resistance in cast aluminum alloy via femtosecond laser induced periodic surface structures and surface hardening layer, Appl. Surf. Sci. 636 (2023), 157866.
[27] Y. Xing, Z. Wu, J. Yang, X. Wang, L. Liu, LIPSS combined with ALD MoS2 nano-coatings for enhancing surface friction and hydrophobic performances, Surf. Coat. Technol. 385 (2020), 125396.